International Journal of Minerals, Metallurgy and Materials
Volume 22, Number 10, October 2015, Page 1067
DOI: 10.1007/s12613-015-1169-9

Comparison of corrosion and oxygen evolution behaviors between cast and rolled Pb–Ag–Nd anodes

Xiao-cong Zhong, Xiao-ying Yu, Zheng-wei Liu, Liang-xing Jiang, Jie Li, and Ye-xiang Liu

School of Metallurgy and Environment, Central South University, Changsha 410083, China
(Received: 3 August 2014; revised: 23 September 2014; accepted: 4 November 2014)

Abstract: The corrosion and oxygen evolution behaviors of cast and rolled Pb–Ag–Nd anodes were investigated by metalloscopy, environmental scanning electron microscopy, X-ray diffraction analysis, and various electrochemical measurements. The rolled anode exhibits fewer interdendritic boundaries and a dispersed distribution of Pb–Ag eutectic mixtures and Nd-rich phases in its cross-section. This feature inhibits rapid interdendritic corrosion into the metallic substrate along the interdendritic boundary network. In addition, the anodic layer formed on the rolled anode is more stable toward the electrolyte than that formed on the cast anode, reducing the corrosion of the metallic substrate during current interruption. Hence, the rolled anode has a higher corrosion resistance than the cast anode. However, the rolled anode exhibits a slightly higher anodic potential than the cast anode after 72 h of galvanostatic polarization, consistent with the larger charge transfer resistance. This larger charge transfer resistance may result from the oxygen-evolution reactive sites being blocked by the adsorption of more intermediates and oxygen species at the anodic layer/electrolyte interfaces of the rolled anode than at the interfaces of cast anode.

Keywords: lead–silver alloys; anode materials; rolling; corrosion resistance; impedance

1. Introduction

Pb–Ag alloys have been widely used as anodes in the zinc electrowinning industry since their first application in 1909 [1]. The alloying addition of Ag has been demonstrated to decrease the over-potential of oxygen evolution reaction (OER) [2–3], increase the compactness of anodic layer [4], and reduce the corrosion rate [5–6]. However, the Ag addition cannot significantly reduce the creep of lead alloys [7], thus, Pb–Ag anodes are observed to be relatively weak and ductile [1], which result in cracks in the adherent PbO_2 layer and exposing the fresh anode surfaces, leading to the further corrosion. Therefore, alloying elements such as Ca [8], Sr, and Co [9] have been added to improve the mechanical properties of Pb–Ag anodes.

In addition to the variation of alloying components, mechanical deformation is also an effective method for improving the performance of Pb–Ag anodes. Rolled Pb–Ag anodes have been reported to exhibit higher corrosion resistance and lower anodic polarization compared to the cast anodes [5]. According to the Ref. [10], alloying components and plastic deformation improve the electrochemical properties and corrosion resistance through the same mechanism as modification of the alloy microstructure. Some authors [7,10–11] have pointed out that the rolling process induced the deformation of cast grain structure, resulted in uniform and fine grains with less segregation, and eliminated cracks, defects, and pores.

In our previous works [12–13], the effects of Nd on the electrochemical performance of Pb–Ag anodes were studied. It was observed that the addition of Nd reduced the corrosion rate and oxygen evolution over-potential of Pb–Ag anodes. In this study, to further investigate the influence of rolling process on Pb–Ag–Nd anodes, the corrosion resistance and OER behavior of cast and rolled Pb–Ag–Nd anodes were investigate and compared.

The metallographic structures, anodic layers, corrosion morphology, and OER of cast and rolled anodes were studied comparatively in this research. A correlation between the

Corresponding author: Liang-xing Jiang E-mail: lxjiang@csu.edu.cn

microstructure and corrosion/OER behavior was proposed on the basis of morphology observations, X-ray characterization, and various electrochemical measurements, such as galvanostatic polarization, potential decay, AC impedance measurements, and Tafel analysis.

2. Experimental

2.1. Electrodes and experimental cell

Cast and rolled Pb–Ag–Nd alloys (0.49wt% Ag and 0.03wt% Nd) were provided by Yuguang Gold & Lead Co., Ltd., China. The raw alloy materials were wire-cut into cuboids of 10 mm × 10 mm × 7 mm. A conductive copper wire was welded to one end of the cuboid piece before it was mounted in a Teflon holder with an exposed geometric area of 1.0 cm^2. All electrochemical measurements were conducted in a three-electrode system with 1.63 $mol \cdot L^{-1}$ H_2SO_4 solution as the electrolyte. The temperature of the test system was controlled at (35 ± 1)°C using a thermostat. A Pt plate with an area of 4 cm^2 and a Hg/Hg_2SO_4/0.1 $mol \cdot L^{-1}$ K_2SO_4 electrode were used as the counter and reference electrodes, respectively. All potentials shown in this study were stated relative to this reference electrode. Each electrode was gradually abraded with SiC paper from 400 grit to 1500 grit and subsequently washed with deionized water before each electrochemical measurement. All electrochemical measurements were performed using an electrochemical workstation (1470 E, Solartron Analytical, UK).

2.2. Measurements

The cast and rolled Pb–Ag–Nd alloys were gradually abraded with SiC paper from 400 grit to 1500 grit and then polished with ultrafine alumina (<0.1 μm). They were subsequently etched with a solution of glacial acetic acid and hydrogen peroxide (3:1, molar ratio). The metallographic structures of the cast and rolled Pb–Ag–Nd alloys were observed by metalloscopy (MeF3A, Leica, Germany). For the rolled Pb–Ag–Nd alloy, both the longitudinal plane and cross-section were observed separately.

Galvanostatic polarization tests were conducted for 72 h at 500 $A \cdot m^{-2}$ in 1.63 $mol \cdot L^{-1}$ H_2SO_4 solution; the anodes were subsequently taken out, washed with deionized water, and dried for 8 h at 80°C. The morphologies of the anodic layers were observed with environmental scanning electron microscopy (ESEM, Quanta-200, FEI, The Netherlands). Moreover, a X-ray diffractometer (D/max 2500, Rigaku Co, Japan) equipped with a Cu K_α radiation source was used to identify the phase composition of the anodic layers. In addition, after the anodic layers were removed, the morphologies of the metallic substrates were also observed.

The corrosion rates of the cast and rolled anodes during 72 h galvanostatic polarization at 500 $A \cdot m^{-2}$ were determined by the weight-loss method. The detailed procedures have been reported elsewhere [14]. The stability of the anodic layers toward electrolyte was analyzed by potential decay tests, which were performed by recording the open-circuit potential after 72 h of polarization at 500 $A \cdot m^{-2}$.

Electrochemical impedance spectroscopy (EIS) measurements were used to investigate the OER dynamics. EIS measurements were conducted after 72 h of galvanostatic polarization. In each EIS measurement, the bias DC potential was the same as the anodic potential measured just before the EIS measurement. The amplitude of the AC signal was 5 mV. The frequency range was from 0.1 Hz to 100 kHz. The impedance data were fitted to an electrical equivalent circuit (EEC) using the Zsimpwin program. The best fit was obtained by minimizing χ^2 (chi squared), which could characterize the accuracy of fitting result.

As quasi-state potentiodynamic measurements, Tafel tests were conducted when the anodic reaction reached a steady state. In this study, both forward and backward potential sweeps were performed after 72 h of galvanostatic polarization. The potential sweep range was between 1.20 V and 1.50 V, and the sweep rate was 0.166 $mV \cdot s^{-1}$.

3. Results and discussion

3.1. Metallographic structure

The performance of metallic materials is determined by their microstructures [15]. Therefore, lead-based anodes with desired corrosion resistance and oxygen evolution reactivity can be obtained by tailoring their microstructures, either through the optimization of alloying elements or through the plastic deformation. To understand the interrelation between the microstructure and corrosion behavior of cast and rolled Pb–Ag–Nd anodes, the microstructures of these two alloys were observed, as shown in Fig. 1.

Because the cast anodes were line-cut from a large cast ingot, the structure of cast alloy could be inferred to be isotropic on a small scale. Therefore, only one micrograph of the cast Pb–Ag–Nd anode is displayed in Fig. 1(a). The as-cast microstructure exhibits a typical cellular array, featuring a Pb-rich matrix (α-phase, the solid solution of Ag or Nd in Pb) with Pb–Ag eutectic mixtures located in the interdendritic boundaries. The Pb-rich matrix and the interdendritic eutectic mixture are indicated by the light regions and the dark regions, respectively. In addition, Nd tends to

form intermetallic compounds with Pb (Nd-rich phases). These Nd-rich phases, indicated by tiny dark dots and large dark regions, are observed in the Pb-rich matrix and interdendritic boundaries.

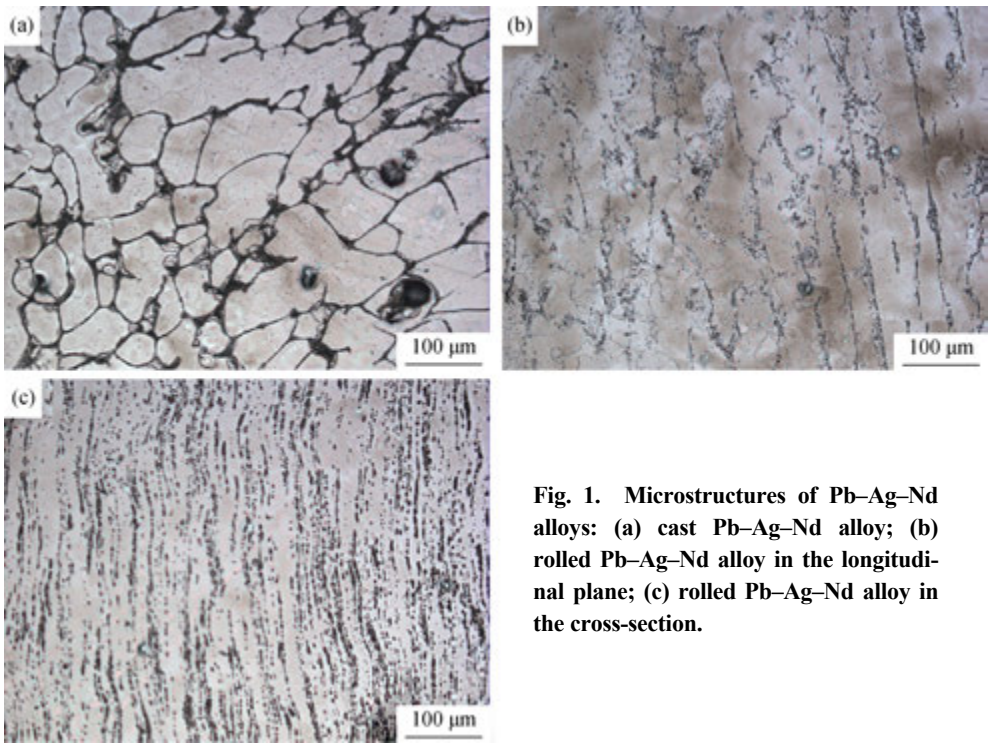

Fig. 1. Microstructures of Pb–Ag–Nd alloys: (a) cast Pb–Ag–Nd alloy; (b) rolled Pb–Ag–Nd alloy in the longitudinal plane; (c) rolled Pb–Ag–Nd alloy in the cross-section.

The hot-rolled Pb–Ag–Nd alloys exhibit the directional macrostructures along the rolling direction. The longitudinal-section microstructure of the rolled anode in Fig. 1(b) indicates that the original cellular array is broken up by the rolling process. Consequently, the eutectic mixtures and Nd-rich phases are distributed discontinuously and dispersedly. The interdendritic boundaries become vague and dispersed. In the cross-section as shown in Fig. 1(c), the microstructure exhibits a lamellar structure. The lamella of the eutectic mixture and Nd-rich constituents segment the Pb-rich matrix layer-by-layer, resulting in a more homogenous and uniform microstructure of the rolled anode.

3.2. Corrosion behavior

(1) Corrosion rates

Table 1 shows the average corrosion rates of the cast and rolled anodes during 72 h of galvanostatic polarization. The rolled anode exhibits a slightly lower corrosion rate. The reason for this lower rate was revealed by the morphologies of the anodic layers and metallic substrates detailed below.

(2) Morphology of the anodic layer

The morphologies of the anodic layers formed by the 72 h of galvanostatic polarization are shown in Fig. 2. The anodic layers on both the cast and rolled anodes exhibit loose surfaces with a typical coral structure. Several holes are distributed on the anodic films, which are mainly produced by the impact of oxygen bubbles. Because of the long duration of polarization, the surface morphologies of the two anodes do not exhibit obvious differences.

Table 1. Corrosion rates of cast and rolled Pb–Ag–Nd anodes during 72 h of galvanostatic polarization $g \cdot m^{-2} \cdot h^{-1}$

Anodes	Test 1	Test 2	Test 3	Average value
Cast anode	3.10	3.02	3.25	3.12
Rolled anode	2.91	2.85	2.88	2.88

(3) Composition of the anodic layer

The X-ray diffraction (XRD) patterns of the anodic layers of the cast and rolled Pb–Ag–Nd anodes after 72 h of galvanostatic polarization are shown in Fig. 3. The anodic layers formed on the two anodes both consist primarily of $PbSO_4$ and PbO_2. The intensities of $PbSO_4$ and PbO_2 peaks in the pattern of the rolled anode are higher than those of the cast anode. This increased intensity is primarily attributed to the thicker anodic layer of the rolled anode. Notably, Pb peaks appear in XRD patterns of both anodes. The presence of Pb peaks indicates that the anodic layer is relatively thin and incompact. Comparatively, the XRD pattern of rolled anode shows less intense Pb peaks, demonstrating that the anodic layer on the rolled anode is slightly thicker and more compact.

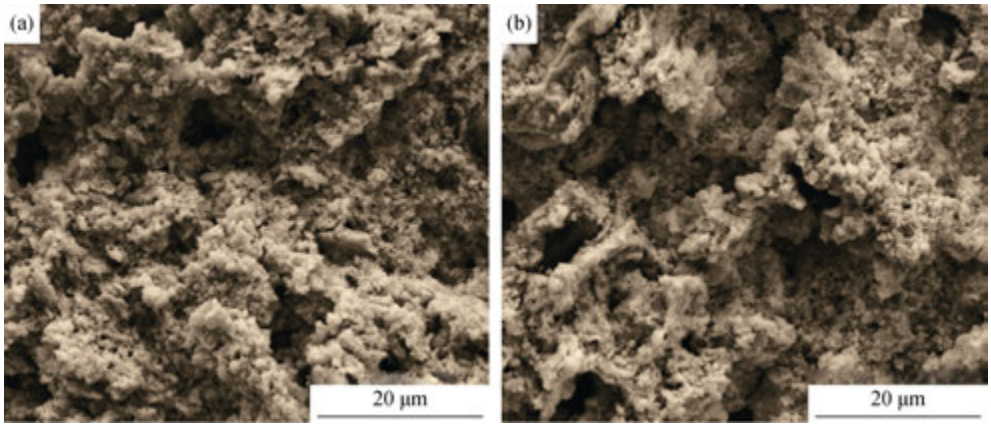

Fig. 2. Morphologies of the anodic layers on the cast (a) and rolled (b) Pb–Ag–Nd anodes formed through 72 h of galvanostatic polarization.

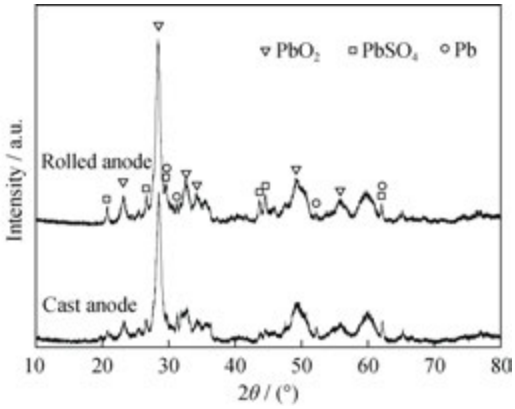

Fig. 3. XRD patterns of the anodic layers on the cast and rolled Pb–Ag–Nd anodes.

(4) Morphology of the metallic substrate

Unlike the morphologies of the anodic layers, the morphologies of the metallic substrates of the cast and rolled anodes differ substantially after the 72-h polarization, as shown in Fig. 4. The substrate of the cast anode exhibits several wide and deep cracks around the Pb-rich matrix, exactly corresponding to the interdendritic boundaries shown in Fig. 1(a). In addition, corrosion holes, which are ascribed to the corrosion of Nd-rich dispersed phases or to the presence of defects such as pores and cracks, also emerge in the Pb-rich matrix. Therefore, the corrosion of the cast anode exhibits clear traits of interdendritic corrosion. The corrosion preferentially occurs on these chemically active regions. In the case of the cast alloys, the corrosion readily occurs in the inner part of the metallic substrates along the interdendritic boundary network, which may lead to the early piercing and failure of the cast anode.

In contrast, the corrosion substrate of the rolled Pb–Ag–Nd anode is intact without any cracks. The difference in the morphology of the corrosion substrate can be explained by the lamellar structure shown in Fig. 1(c). The interdendritic boundaries and Nd-rich phases in the cross-section of the rolled alloys are distributed evenly, dispersedly, and discontinuously. Without the intact interdendritic boundary network in the cross-section, the rolled anode tends to undergo the homogeneous corrosion. The corrosion could only extend further into the metallic substrate in a layer-by-layer fashion.

In summary, the rolled Pb–Ag–Nd metallic substrate exhibits the greater corrosion resistance through two

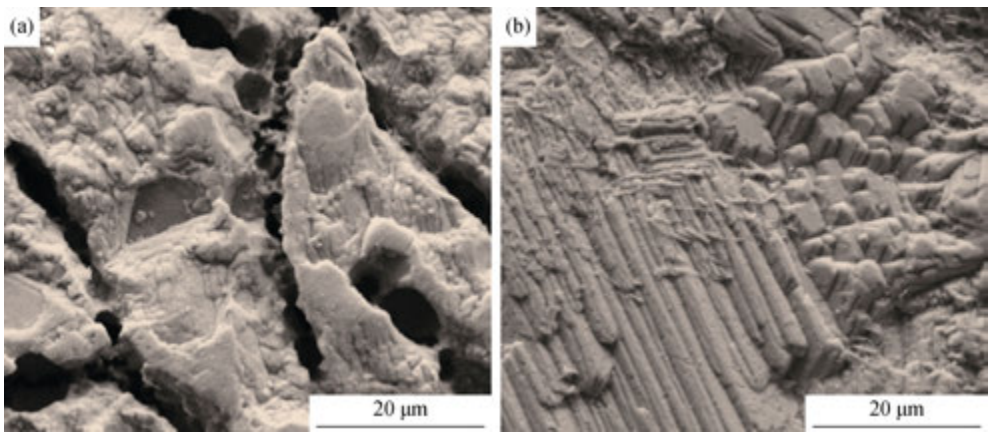

Fig. 4. Morphologies of the metallic substrates of cast (a) and rolled (b) Pb–Ag–Nd anodes after removal of the anodic layers.

mechanisms. One mechanism relies on its fewer interdendritic boundaries, which are more chemically active than the grain itself (Pb matrix) [16]. The other mechanism is related to the absence of an intact interdendritic boundary network in the cross-section.

(5) Potential decay

Potential decay tests, also called self-depassivation tests, were used to investigate the transformation of different phase compositions of anodic layers and the stability of the anodic protective layer toward the electrolyte when the cell current was switched off [17–18]. Fig. 5 shows the open-circuit potential of the anodes after 72 h of galvanostatic polarization.

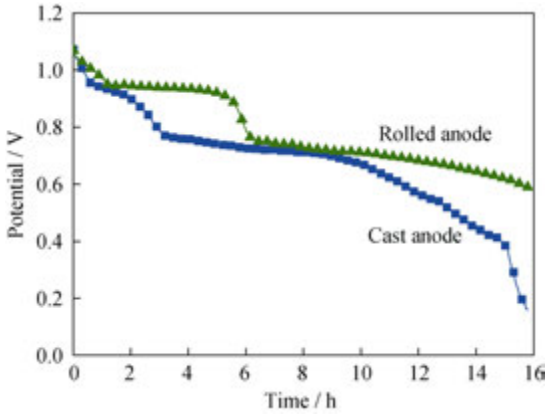

Fig. 5. Open-circuit potential variation of the 72 h-polarized cast and rolled Pb–Ag–Nd anodes during potential decay tests.

The potentials of the two anodes quickly decrease from the working potential to approximately 0.95 V at the beginning of the decay tests. During this period, the oxygen species absorbed on the anodic layers are removed [19]. The time required for the removal of oxygen species in the case of the rolled anode is twice that required in the case of the cast anode. Thus, more oxygen species may be adsorbed onto the surface layer of the rolled anode. Next, a potential plateau occurs at approximately 0.95 V. According to the Ref. [18], the reduction of lead(IV) oxide to lead(II) sulfate on the anode couples with the oxidation of metallic lead to lead(II) sulfate, thereby generating a mixed potential that corresponds to the potential plateau. For the rolled anode, the potential plateau lasts approximately 3.7 h, whereas that of the cast anode lasts only approximately 1.2 h. The duration of the potential plateau is determined by the amount of PbO_2 and by the kinetics of the transformation reaction. Because the two reactions are driven by the potential gap between two electrochemical couples and no current is present in the circuit, calculating the amount of the corresponding reactants is difficult. The longer potential plateau for the rolled anode may be caused primarily by its thicker anodic layer and by the presence of more PbO_2, as inferred from the XRD analysis results. It may also be caused by a slower transformation rate. The more intact anodic layer on the rolled anode may inhibit the transfer of SO_4^{2-} and H_2O into the anodic layer, which may further explain its longer potential plateau.

After the first potential plateau, the potentials for both the cast and rolled anodes decrease rapidly again and then exhibit a long-lasting and slow potential decay. In the potential range from 0.75 V to 0.15 V, the potential is a mixture of the potential of such electrochemical couples as tetra-PbO_n ($1 < n < 2$)/$PbSO_4$, PbO/Pb, and Pb/$PbSO_4$. During the transformation of different phase compositions on the anodic layer, some cracks may emerge because of the difference in mole volumes among the different phase compositions, leading to etching and dissolution of the metallic substrate. As shown in Fig. 5, the potential of the cast anode decreases drastically from 0.40 V to 0.15 V, indicating the formation of cracks via the aforementioned mechanism.

In the potential range shown in Fig. 5, the potential decay of the rolled anode is much slower. It is concluded that the anodic layer formed on the rolled anode is thicker or more intact, helping to protect the metallic substrates. A slower potential decay indicates greater stability of the rolled anode toward the electrolyte under the condition of current interruption. With greater corrosion resistance of metallic substrate and greater stability toward the electrolyte, the rolled anode has a higher corrosion resistance during service, consistent with its lower corrosion rate.

3.3. Oxygen evolution behavior

(1) AC impedance

As previously mentioned, the over-potential of OER critically affects the energy consumption during zinc electrowinning. In addition, the OER of anode fundamentally affects the corrosion process. Therefore, the oxygen evolution behaviors of cast and rolled anodes were compared in this study.

The EIS technique has been widely adopted to investigate the OER of metallic oxide electrodes [17,20]. To further study the kinetics of OER and anodic film structures, EIS measurements were conducted in this study. Before the EIS measurements, the anodic potentials were measured at the end of 72 h of galvanostatic polarization. The anodic potential of the cast anode was 1.35 V, and that of the rolled anode was 1.37 V, approximately 20 mV higher.

Fig. 6 shows the typical Nyquist plots for the cast and rolled Pb–Ag–Nd anodes. The complex plane exhibits only

one capacitance over the whole frequency domain, indicating that the charge transfer resistance of oxygen evolution is in parallel with the double-layer capacitance. An obvious inductance (L) is observed at high frequencies, which is attributed to the charge relaxation on electroactive materials with heterogeneity or energy disorder.

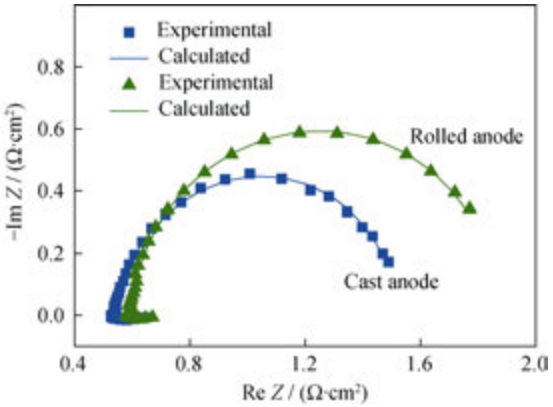

Fig. 6. Nyquist plots of the cast and rolled Pb–Ag–Nd anodes after 72 h of galvanostatic polarization. The bias DC potential is 1.35 V for the cast anode and 1.37 V for the rolled anode.

According to the Ref. [21], because of the irreversible character of OER with one state variable in addition to the electrode potential, the faradaic impedance (Z_F) of OER can be expressed as Eq. (1).

$$Z_F = R_{ct} + \frac{R_a}{1 + j\omega R_a C_a} \tag{1}$$

where ω is the angular frequency, R_{ct} the charge transfer resistance of OER, and R_a and C_a the equivalent resistance and the pseudo-capacitance associated with the adsorption of intermediates, respectively. Given the existence of an anodic layer, a combination factor (R_fC_f) is sometimes added to account for the capacitive response of oxide layer, where R_f and C_f indicate the resistance and capacitance of the oxide layer, respectively.

The use of a constant phase element (CPE) is a good approach for the study of solid electrodes with different degrees of surface roughness, physical nonuniformity, or a nonuniform distribution of surface reaction sites [22]. The CPE was used instead of capacitance (C) to fit the experimental data for the double-layer capacitance (C_{dl}). The impedance of CPE (Z_{CPE}) is expressed as Eq. (2).

$$Z_{CPE} = \frac{1}{Q(j\omega)^n} \tag{2}$$

where Q represents the capacity parameter, $F \cdot cm^{-2} \cdot s^{(n-1)}$, and n accounts for the deviation from the ideal behavior ($n = 1$ for a perfect capacitor). Other authors [23] have proposed that C_{dl} is coupled with the uncompensated solution resistance (R_s) and with the charge transfer resistance (R_{ct}) according to the following equation.

$$Q = (C_{dl})^n \left[(R_s)^{-1} + (R_{ct})^{-1} \right]^{(1-n)} \tag{3}$$

Therefore, C_{dl} was calculated using the Q values obtained from the EEC approximation via Eq. (3). The simulated patterns and parameters derived by fitting the impedance data of the cast and rolled Pb–Ag–Nd anodes are presented in Fig. 6 and Table 2, respectively. In the simulation of the cast Pb–Ag–Nd anode, the calculated values based on the EEC illustrated in Fig. 7(a) are in good agreement with the experimental data ($\chi^2 = 1.35 \times 10^{-3}$). However, with regard to the rolled Pb–Ag–Nd anode, only when the layer impedance loop (R_fC_f) is added into the circuit, as shown in Fig. 7(b), a satisfactory approximation is obtained ($\chi^2 = 7.54 \times 10^{-4}$).

Table 2. Equivalent circuit parameters for the cast and rolled Pb–Ag–Nd anodes

Anodes	R_s / (Ω·cm²)	C_f / (F·cm^{-2})	R_f / (10^{-2}Ω·cm²)	C_{dl} / (10^{-2}F·cm^{-2})	R_{ct} / (Ω·cm²)	C_a / (F·cm^{-2})	R_a / (Ω·cm²)
Cast	0.544	—	—	4.54	0.751	0.113	0.226
Rolled	0.596	0.399	1.35	5.15	1.070	0.311	0.186

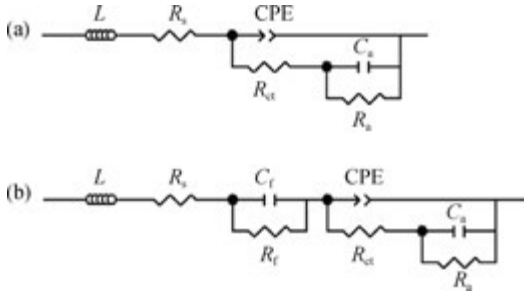

Fig. 7. Electrical equivalent circuits used to fit the impedance data shown in Fig. 6: (a) cast Pb–Ag–Nd anode; (b) rolled Pb–Ag–Nd anode.

As shown in Table 2, the rolled Pb–Ag–Nd anode also has a higher double-layer capacitance (C_{dl}) than the cast Pb–Ag–Nd anode. This result is consistent with its larger C_a value and smaller R_a value, demonstrating that the adsorption intermediate, $PbO^{\bullet}(OH)_2 \cdots (OH^{\circ})$, is more readily formed at the anodic layer/solution interface of the rolled anode. However, the charge transfer resistance (R_{ct}) for the OER of the rolled Pb–Ag–Nd anode is larger than that of the cast anode, indicating that the anodic layer/solution interfaces on the rolled anode are less favorable to charge transfer. Higher R_{ct} and lower R_a values result in more adsorption

intermediates and oxygen species at the anodic layer/solution interface on the rolled anode, which is consistent with the analysis of the potential decay tests. These adsorption intermediates and oxygen species may block the reactive sites for OER, which can explain the slightly higher anodic potential of the rolled anode.

(2) Tafel analysis

To further explore the OER dynamics on the cast and rolled anodes, the Tafel analyses were conducted after 72 h of polarization. The results shown in Fig. 8 were obtained via the backward potential sweeps. All experimental Tafel curves show a deviation from linearity at high over-potential, which requires correction for the ohmic drop expressed by Eq. (4), as proposed elsewhere [24].

$$E_{\text{eff}} = E_{\text{appl}} - IR \tag{4}$$

where E_{eff} and E_{appl} represent the effective and applied potential of anode, respectively, and IR represents the ohmic drop of the anodic process. However, the resistance of the anodic film is very small, as demonstrated in the EIS analysis. Hence, R can be approximated by the R_s values reported in Table 2.

As shown in Fig. 8, after the ohmic-drop correction, both curves feature two Tafel slopes obtained separately by linear fitting of the low and high over-potential regions. The results are listed in Table 3. At low over-potential regions, the Tafel slopes for the cast and rolled anodes are 114 and 101 mV dec^{-1}, respectively. However, the Tafel slopes at high over-potential regions increase to 172 and 181 mV dec^{-1} for the cast and rolled anodes, respectively, which are quite similar to the OER Tafel slope reported for β-PbO_2 in Ref. [24]. For the lead dioxide electrode, when the Tafel coefficient (b) is near 120 mV·dec^{-1}, the formation and adsorption of the intermediate, $PbO^{\bullet}(OH)_2\cdots(OH^{\circ})$, are suggested to be the rate-determining steps [25–26]. In this respect, at low over-potentials, the OER occurring on the cast and rolled anodes is controlled by both the formation and adsorption of the intermediates. The lower slope for the rolled anode may be related to its smaller R_a, as shown in Table 2. At the high over-potential regions, the slopes increase, which may be attributed to the influence of partially evolved O_3 [22]. However, other studies attributed this phenomenon to the micro-porous essence of lead-based anodes. At higher over-potential regions, the mass and charge transfer may become insufficient because of the longer transfer distance and the blocking of the micro-pores by increasingly evolved O_2 [27]. Together, the analysis of the potential decay and the EIS results suggest that the higher Tafel slopes of the cast and rolled anodes at high over-potentials may result from the blocking of interfaces by the intermediates and oxygen species. Because of the absorption of more intermediates and oxygen species on the rolled anode, its slope is larger than that of the cast anode, which further explains the higher anodic potentials of the rolled anode.

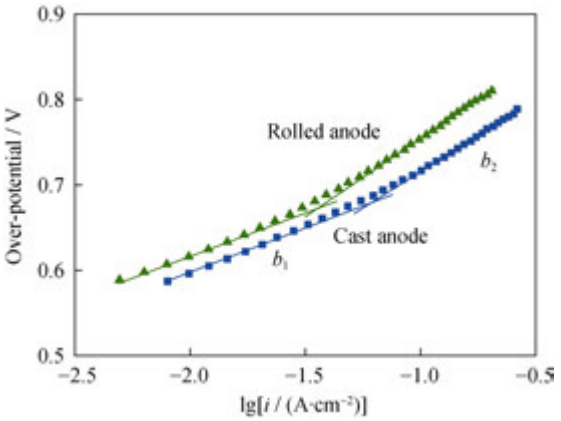

Fig. 8. Tafel curves of the cast and rolled Pb–Ag–Nd anodes in 1.63 mol/L H_2SO_4 solution at 35°C, where b_1 and b_1 represent the Tafel slopes at low and high over-potential regions, respectively.

Table 3. OER dynamic parameters of the cast and rolled Pb–Ag–Nd anodes obtained from the Tafel curves shown in Fig. 8

Anode	b_1 / (mV·dec^{-1})	b_1 / (mV·dec^{-1})
Cast anode	114	172
Rolled anode	101	181

Notably, different from the previously published results [5], it was here reported that the rolled anodes exhibited a slightly larger anodic potential after 72 h of galvanostatic polarization. This increased anodic potential might be related to the polarization time. As mentioned in the Ref. [7], the rolled anodes required a longer time to form a stable anodic layer and reach a stable anodic potential. With longer polarization times (on the order of months), the rolled anode might exhibit a lower anodic potential. Therefore, the OER behavior of the rolled anode during longer polarization times should be investigated in future work.

4. Conclusions

(1) The rolling process breaks up the cellular array of the cast Pb–Ag–Nd alloys, resulting in a lamellar structure with dispersed eutectic mixtures and Nd-rich phases. Without an intact and continuous interdendritic boundary network in the cross-section, the rolled Pb–Ag–Nd anode undergoes the homogeneous corrosion instead of rapid corrosion into the

metallic substrate along the interdendritic boundary network.

(2) The anodic layer formed on the rolled anode exhibits the greater stability toward the electrolyte, which is attributed to the anodic layer being thicker or more intact. Therefore, the rolled anode exhibits higher corrosion resistance.

(3) The rolled Pb–Ag–Nd anode exhibits a slightly higher anodic potential compared to that of the cast Pb–Ag–Nd anode. It is attributed this higher potential to the adsorption of more intermediates and oxygen species at the anodic layer/solution interface, which severely blocks the reactive sites for the OER.

Acknowledgements

This work was financially supported by the National Natural Science Foundation of China (Nos. 51204208 and 51374240), the Natural Science Foundation of Hunan Provincial, China (No. 13JJ1003), and the Fundamental Research Funds for the Central Universities of Central South University (No. 2014zzts028).

References

[1] R.H. Newnham, Corrosion rates of lead based anodes for zinc electrowinning at high current densities, *J. Appl. Electrochem*., 22(1992), No. 2, p. 116.

[2] W. Zhang, C.Q. Tu, Y.F. Chen, H. Georgeos, and L. Xiao, Effect of MnO_4^- and silver content on electrochemical behaviour of Pb–Ag alloy anodes during potential decay periods, *Trans. Nonferrous Met. Soc. China*, 23(2013), No. 7, p. 2174.

[3] J.J. McGinnity and M.J. Nicol, The role of silver in enhancing the electrochemical activity of lead and lead–silver alloy anodes, *Hydrometallurgy*, 144–145(2014), p. 133.

[4] M. Tunnicliffe, F. Mohammadi, and A. Alfantazi, Polarization behavior of lead–silver anodes in zinc electrowinning electrolytes, *J. Electrochem. Soc.*, 159(2012), No. 4, p. C170.

[5] M. Petrova, Z. Noncheva, Ts. Dobrev, St. Rashkov, N. Kounchev, D. Petrov, St. Vlaev, V. Mihnev, S. Zarev, L. Georgieva, and D. Buttinelli, Investigation of the processes of obtaining plastic treatment and electrochemical behaviour of lead alloys in their capacity as anodes during the electroextraction of zinc: I. Behaviour of Pb–Ag, Pb–Ca and Pb–Ag–Ca alloys, *Hydrometallurgy*, 40(1996), No. 3, p. 293.

[6] H.T. Yang, H.R. Liu, Y.C. Zhang, B.M. Chen, Z.C. Guo, and R.D. Xu, Properties of a new type Al/Pb–0.3%Ag alloy composite anode for zinc electrowinning, *Int. J. Miner. Metall. Mater.*, 20(2013), No. 10, p. 986.

[7] A. Felder and R.D. Prengaman, Lead alloys for permanent anodes in the nonferrous metals industry, *JOM*, 58(2006), No. 10, p. 28.

[8] S.P. Zhong, Y.Q. Lai, L.X. Jiang, Z.L. Tian, J.F. Li, and Y.X. Liu, Anodization behavior on Pb–Ag–Ca–Sr alloy during zinc electrowinning, *Chin. J. Nonferrous Met.*, 18(2008), No. 7, p. 1342.

[9] Y.C. Zhang, B.M. Chen, and Z.C. Guo, Electrochemical properties and microstructure of Al/Pb–Ag and Al/Pb–Ag–Co anodes for zinc electrowinning, *Acta Metall. Sin.*, 27(2014), No. 2, p. 331.

[10] St. Rashkov, Y. Stefanov, Z. Noncheva, M. Petrova, Ts. Dobrev, N. Kunchev, D. Petrov, St. Vlaev, V. Mihnev, S. Zarev, L. Georgieva, and D. Buttinelli, Investigation of the processes of obtaining plastic treatment and electrochemical behaviour of lead alloys in their capacity as anodes during the electroextraction of zinc: II. Electrochemical formation of phase layers on binary Pb–Ag and Pb–Ca, and ternary Pb–Ag–Ca alloys in a sulphuric-acid electrolyte for zinc electroextraction, *Hydrometallurgy*, 40(1996), No. 3, p. 319.

[11] M. Clancy, C.J. Bettles, A. Stuart, and N. Birbilis, The influence of alloying elements on the electrochemistry of lead anodes for electrowinning of metals: a review, *Hydrometallurgy*, 131–132(2013), p. 144.

[12] B. Hong, L.X. Jiang, X.J. Lü, H.F. Ni, Y.Q. Lai, J. Li, and Y.X. Liu, Influence of Nd on Pb–Ag alloy anode for zinc electrowinning, *Chin. J. Nonferrous Met.*, 22(2012), No. 4, p. 1126.

[13] X.C. Zhong, J.F. Gui, X.Y. Yu, F.Y. Liu, L.X. Jiang, Y.Q. Lai, J. Li, and Y.X. Liu, Influence of alloying element Nd on the electrochemical behavior of Pb–Ag anode in H_2SO_4 solution, *Acta Phys. Chim. Sin.*, 30(2014), No. 3, p. 492.

[14] A. Hrussanova, L. Mirkova, Ts. Dobrev, and S. Vasilev, Influence of temperature and current density on oxygen overpotential and corrosion rate of Pb–Co_3O_4, Pb–Ca–Sn, and Pb–Sb anodes for copper electrowinning: Part I, *Hydrometallurgy*, 72(2004), No. 3–4, p. 205.

[15] D.A.J. Rand, D.P. Boden, C.S. Lakshmi, R.F. Nelson, and R.D. Prengaman, Manufacturing and operational issues with lead-acid batteries, *J. Power Sources*, 107(2002), No. 2, p. 280.

[16] K.D. Ralston and N. Birbilis, Effect of grain size on corrosion: a review, *Corrosion*, 66(2010), No. 7, p. 075005.

[17] W. Zhang and G. Houlachi, Electrochemical studies of the performance of different Pb–Ag anodes during and after zinc electrowinning, *Hydrometallurgy*, 104(2010), No. 2, p. 129.

[18] L. Cifuentes, E. Astete, G. Crisóstomo, J. Simpson, G. Cifuentes, and M. Pilleux, Corrosion and protection of lead anodes in acidic copper sulphate solutions, *Corros. Eng. Sci. Technol.*, 40(2005), No. 4, p. 321.

[19] M. Mohammadi, F. Mohammadi, G. Houlachi, and A. Alfantazi, The role of electrolyte hydrodynamic properties on the performance of lead-based anodes in electrometallurgical processes, *J. Electrochem. Soc.*, 160(2013), No. 3, p. E27.

[20] C.J. Yang, Y. Ko, and S.M. Park, Fourier transform electrochemical impedance spectroscopic studies on anodic reaction of lead, *Electrochim. Acta*, 78(2012), p. 615.

[21] S. Palmas, A.M. Polcaro, F. Ferrara, J. Ruiz Rodriguez, F. Delogu, C. Bonatto-Minella, and G. Mulas, Electrochemical

performance of mechanically treated SnO_2 powders for OER in acid solution, *J. Appl. Electrochem.*, 38(2008), No. 7, p. 907.

[22] D.V. Franco, L.M.D. Silva, W.F. Jardim, and J.F.C. Boodts, Influence of the electrolyte composition on the kinetics of the oxygen evolution reaction and ozone production processes, *J. Brazil. Chem. Soc.*, 17(2006), No. 4, p. 746.

[23] G.J. Brug, A.L.G. van den Eeden, M. Sluyters-Rehbach, and J.H. Sluyters, The analysis of electrode impedances complicated by the presence of a constant phase element, *J. Electroanal. Chem. Interfacial Electrochem.*, 176(1984), No. 1–2, p. 275.

[24] J.C.K. Ho, G. Tremiliosi Filho, R. Simpraga, and B.E. Conway, Structure influence on electrocatalysis and adsorption of intermediates in the anodic O_2 evolution at dimorphic α-and β-PbO_2, *J. Electroanal. Chem.*, 366(1994), No. 1-2, p. 147.

[25] Y.Q. Lai, Y. Li, L.X. Jiang, W. Xu, X.J. Lv, J. Li, and Y.X. Liu, Electrochemical behaviors of co-deposited Pb/Pb–MnO_2 composite anode in sulfuric acid solution: Tafel and EIS investigations, *J. Electroanal. Chem.*, 671(2012), p. 16.

[26] Y.Q. Lai, Y. Li, L.X. Jiang, X.J. Lv, J. Li, and Y.X. Liu, Electrochemical performance of a Pb/Pb–MnO_2 composite anode in sulfuric acid solution containing Mn^{2+}, *Hydrometallurgy*, 115–116(2012), p. 64.

[27] P. Shrivastava and M.S. Moats, Ruthenium palladium oxide-coated titanium anodes for low-current-density oxygen evolution, *J. Electrochem. Soc.*, 155(2008), No. 7, p. E101.